REDD1 Ablation Attenuates the Development of Renal Complications in Diabetic Mice

Siddharth Sunilkumar,[1] Esma I. Yerlikaya,[1] Allyson L. Toro,[1] William P. Miller,[1] Han Chen,[2] Kebin Hu,[1,3] Scot R. Kimball,[1] and Michael D. Dennis[1]

Diabetes 2022;71:2412–2425 | https://doi.org/10.2337/db22-0402

Chronic hyperglycemia contributes to development of diabetic kidney disease by promoting glomerular injury. In this study, we evaluated the hypothesis that hyperglycemic conditions promote expression of the stress response protein regulated in development and DNA damage response 1 (REDD1) in the kidney in a manner that contributes to the development of oxidative stress and renal injury. After 16 weeks of streptozotocin-induced diabetes, albuminuria and renal hypertrophy were observed in wild-type (WT) mice coincident with increased renal REDD1 expression. In contrast, diabetic REDD1 knockout (KO) mice did not exhibit impaired renal physiology. Histopathologic examination revealed that glomerular damage including mesangial expansion, matrix deposition, and podocytopenia in the kidneys of diabetic WT mice was reduced or absent in diabetic REDD1 KO mice. In cultured human podocytes, exposure to hyperglycemic conditions enhanced REDD1 expression, increased reactive oxygen species (ROS) levels, and promoted cell death. In both the kidney of diabetic mice and in podocyte cultures exposed to hyperglycemic conditions, REDD1 deletion reduced ROS and prevented podocyte loss. Benefits of REDD1 deletion were recapitulated by pharmacological GSK3β suppression, supporting a role for REDD1-dependent GSK3β activation in diabetes-induced oxidative stress and renal defects. The results support a role for REDD1 in diabetes-induced renal complications.

Diabetic nephropathy (DN) is a chronic complication of diabetes that progresses to end-stage renal failure. DN represents a growing socioeconomic and global health burden, with the annual incidence of end-stage renal disease among patients with diabetes reaching 1,016 per million in 2015 (1). The Diabetes Control and Complications Trial demonstrated a key role for hyperglycemia in the development and progression of renal complications (2). However, current therapeutic interventions used in combination with glycemic control have not proven sufficient to halt or reverse DN progression (3,4). This is at least in part due to a deficit in understanding of the specific molecular events that contribute to renal pathology.

Diabetes-associated kidney damage includes functional and structural changes in glomerular cells, including podocytes, mesangial cells, and endothelial cells (5). Podocytes are terminally differentiated epithelial cells that preserve glomerular structure and maintain barrier function by allowing the selective filtration of water and solutes, while preventing large macromolecules like proteins from leaking into the urine (6). Among the changes in renal morphology that are caused by diabetes, a reduced number of podocytes per glomerulus, known as podocytopenia, is the strongest predictor of DN progression (7–9). Podocytopenia is observed in patients with early and late DN (7,8), as well as in animal models of type 1 and type 2 diabetes (9,10). A variety of stressors associated with diabetes, including oxidative stress, inflammation, and endoplasmic reticular stress, contribute to podocytopenia (11). Hyperglycemia-induced reactive oxygen species (ROS) have specifically been shown to decrease podocyte viability by triggering caspase-3–mediated apoptosis (12).

Expression of the stress response protein regulated in development and DNA damage response 1 (REDD1) (also

[1]Department of Cellular and Molecular Physiology, Penn State College of Medicine, Hershey, PA
[2]Transmission Electron Microscopy Core, Penn State College of Medicine, Hershey, PA
[3]Division of Nephrology, Department of Medicine, Penn State College of Medicine, Hershey, PA

Corresponding author: Michael D. Dennis, mdennis@psu.edu

Received 29 April 2022 and accepted 17 August 2022

This article contains supplementary material online at https://doi.org/10.2337/figshare.20503266.

known as DDIT4/RTP801) has been linked to the development of oxidative stress in multiple pathological conditions, including diabetic retinopathy (13–15). Our laboratory demonstrated a critical role for REDD1 in the development of diabetes-induced retinal complications and functional deficits in vision (15–18). Furthermore, clinical intervention with an siRNA targeting REDD1 has shown promise for the improvement of vision in patients suffering from diabetic macular edema (19). REDD1 acts at least in part to promote association of PP2A with Akt, leading to site-specific dephosphorylation of the kinase and reduced Akt-dependent suppression of glycogen synthase kinase 3β (GSK3β) (20). Interplay between REDD1 and GSK3β signaling contributes to the development of hyperglycemia-induced oxidative stress via suppression of the Nrf2 antioxidant response (18). GSK3β hyperactivity is associated with DN progression, and GSK3 inhibitors are currently being pursued as potential therapeutic options (21,22). However, a role for REDD1 in DN has never been investigated. Herein, we examined a role for REDD1 in development of renal complication caused by diabetes.

RESEARCH DESIGN AND METHODS

Animals

Male wild-type (WT) and REDD1 knockout (KO) mice on a B6;129 background (23) were administered 50 mg/kg streptozotocin (STZ) intraperitoneally for five consecutive days to induce diabetes. Control mice received equivalent volumes of sodium citrate vehicle. Diabetic phenotype was confirmed by fasting blood glucose concentrations >250 mg/dL. For examination of a role for GSK3β, C57BL/6J mice (The Jackson Laboratory, Bar Harbor, ME) were administered STZ as described above and then received daily intraperitoneal injections of either VP3.15 (10 mg/kg; MedChemExpress, Monmouth Junction, NJ) or vehicle (10% DMSO, 0.9% NaCl) during the last 3 weeks of diabetes. At 16 weeks of diabetes, mice were euthanized, and terminal urine collection was carried out from the bladder. Both kidneys were removed, weighed, and processed for examination. All procedures adhered to the National Institutes of Health Guide for the Care and Use of Laboratory Animals and were approved by the Penn State College of Medicine Institutional Animal Care and Use Committee.

Urinalysis

Urine protein was separated by SDS-PAGE, transferred to polyvinylidene fluoride membrane, and visualized with reversible protein stain (Thermo Fisher Scientific). Urine creatinine and albumin concentrations were determined with Creatinine (urinary) Colorimetric Assay Kit (Cayman Chemical) and Mouse Albumin ELISA Kit (Eagle Biosciences), respectively.

Histology

Renal sections (6 μm) were cut from 10% formalin-fixed, paraffin-embedded (FFPE) kidneys. Periodic acid-Schiff (PAS) and hematoxylin-eosin (H-E) staining were performed as previously described (9). Immunohistochemical analyses were carried out with ImmPRESS HRP Horse Anti-Rabbit IgG Polymer Detection Kit (Vector Laboratories). Heat-induced antigen retrieval was carried out with citrate buffer (0.01 mol/L, pH 6), and endogenous peroxidase activity was quenched through incubation of sections in BLOXALL Blocking Solution. Sections were then blocked with 2.5% horse serum, incubated overnight with appropriate antibodies (Supplementary Table 1), and detected with 3,3′-diaminobenzidine. Tissue sections were counterstained with H-E, and micrographs were captured with an Olympus BX51 brightfield microscope. Fibronectin or nitrotyrosine immunoreactivity was quantified with ImageJ software. WT-1–positive cells in glomeruli (20 per section) were counted.

Quantification of Morphology

All quantifications were performed in a masked manner and carried out as previously described (24). We evaluated glomerular mesangial expansion and glomerular volume (GV) in sagittal kidney sections by examining 30–50 cortical glomeruli per mouse (five mice per group). The index of the mesangial expansion was defined as ratio of mesangial area to glomerular tuft area. Glomerular area (GA) was quantified with ImageJ and converted to GV with a spherical approximation formula ($GV = 1.2545(GA)^{1.5}$).

Electron Microscopy

Renal cortical tissue (~1 mm^3) from diabetic and nondiabetic WT and REDD1 KO mice was fixed with 2.5% glutaraldehyde and 2% paraformaldehyde in 0.1 mol/L phosphate buffer (pH 7.4), followed by 1% osmium tetroxide in 0.1 mol/L phosphate buffer (pH 7.4) for 1 h. Samples were dehydrated in a graduated series of ethanol and acetone and embedded in LX 112 (Ladd Research Industries, Williston, VT). Thin sections (65 nm) were stained with uranyl acetate and lead citrate and viewed in a JEOL JEM-1400 Transmission Electron Microscope (JEOL USA) located at the Penn State College of Medicine Transmission Electron Microscopy Core (Research Resource Identifier [RRID] SCR_021200).

In Situ Hybridization

REDD1 mRNA was detected with the RNAscope 2.5 HD Assay-RED detection kit and the RNAscope probe Mm-Ddit4 (Advanced Cellular Diagnostics) targeting nucleotides 133–1480 of NM_029083.2. RNA in situ hybridization (ISH) was carried out on 6 μm FFPE kidney sections according to the manufacturer's protocol. Sections were deparaffinized and pretreated with heat and protease before hybridization of REDD1 mRNA probe. Preamplifier, amplifier, and alkaline phosphatase–labeled oligonucleotides were sequentially hybridized followed by application of a chromogenic substrate to produce red punctate dots. Tissue was counterstained with Mayer hematoxylin, and

micrographs were captured with an Olympus BX51 bright-field microscope.

TUNEL

Apoptosis was measured with the DeadEnd fluorometric terminal deoxynucleotidyl transferase dUTP nick end labeling (TUNEL) system assay kit (Promega) according to the manufacturer's instructions. Prior to TUNEL staining, FFPE kidney sections were rehydrated and immunofluorescence staining for WT-1 was carried out. Sections were then fixed in 4% paraformaldehyde and permeabilized with 20 μg/mL Proteinase K and then incubated with TUNEL reaction mixture for 60 min at 37°C in a humidified dark chamber. Kidney sections were subsequently washed with 2× saline-sodium citrate buffer (0.3 mol/L sodium chloride, 0.03 mol/L sodium citrate) and PBS and mounted with VECTASHIELD + DAPI (Vector Laboratories). Images were captured with the Leica SP8 confocal laser microscope with frame-stack sequential scanning.

Cell Culture

Conditionally immortalized human podocytes (CIHP-1) were purchased from Dr. Moin Saleem's laboratory at the University of Bristol (Bristol, U.K.), proliferated at 33°C in 5% CO_2, and then differentiated for 10 days at 37°C in 5% CO_2 (25). Cells were cultured in RPMI-1640 media (Sigma-Aldrich) supplemented with 10% FBS and 1% penicillin/streptomycin. CRISPR/Cas9 genome editing was used to generate a stable CIHP-1 cell line deficient in REDD1 (REDD1 KO) as previously described (26). Cells were exposed to culture medium containing either 30 mmol/L glucose or 5 mmol/L glucose supplemented with 25 mmol/L mannitol as an osmotic control. In specific studies, cells were exposed to medium containing the GSK3 inhibitor VP3.15 (1 μmol/L).

ROS Measurement

Renal lysates were centrifuged at 1,500*g* for 3 min, and the supernatant was exposed to 10 μmol/L 2′,7′-dichlorofluorescein (DCF). Fluorescence (excitation/emission = 504/529 nm) was measured with a SpectraMax M5 plate reader (Molecular Devices, San Jose, CA). Intracellular ROS were assessed in CIHP-1 cultures with a DCFDA Cellular Reactive Oxygen Species Detection Assay Kit (Abcam, Cambridge, U.K.) according to the manufacturer's instructions. Cellular ROS were imaged by confocal microscopy.

Antioxidant Response Element–Luciferase Reporter Assay

Differentiated CIHP-1 WT and REDD1 KO cells were cotransfected with the pRL-CMV *Renilla* luciferase (Promega) and antioxidant response element (ARE)-firefly luciferase (kindly provided by Dr. Jiyang Cai, University of Texas Medical Branch) plasmids combined in a 10:1 ratio using jetPRIME (Polyplus transfection). After 24 h, transfection media were removed, and cells were exposed to hyperglycemic conditions for 48 h. Luciferase activity was measured on a FlexStation 3 (Molecular Devices) with a Dual-Luciferase Assay Kit (Promega).

Viability Assay

WT and REDD1 KO cells were plated at a density of 10^4 cells per well in a 96-well plate in 200 μL culture medium and allowed to adhere overnight at 33°C. Cells were then differentiated for 10 days followed by exposure to hyperglycemic conditions for 0–48 h. Cell viability was determined with the MTT Cell Proliferation Assay Kit (Cayman Chemical, Ann Arbor, MI) following the manufacturer's instructions. Briefly, 10 μL of a 5 mg/mL 3-(4,5-dimethylthiazol-2-yl)-2,5-diphenyltetrazolium bromide (MTT) solution was added to each well. After 4 h incubation, the medium was carefully aspirated, the purple formazan crystals were solubilized, and optical density was measured at 570 nm.

Western Blotting

Total protein was extracted from cells in culture and tissue that was flash frozen in liquid nitrogen. Approximately 20 mg of renal cortical tissue was homogenized in 200 μL of lysis buffer (50 mmol/L Tris [pH 7.4], 150 mmol/L NaCl, 1% NP-40, 0.5% Na-deoxycholate, 1% protease-phosphatase inhibitors) and protein concentrations were estimated with DC protein assay (Bio-Rad Laboratories). Protein from cell lysates or kidney homogenates were combined with Laemmli buffer, boiled, and fractionated with use of Criterion precast 4–20% gels (Bio-Rad Laboratories). Proteins were transferred to polyvinylidene fluoride membrane, reversibly stained for assessment of protein loading, blocked in 5% milk in Tris-buffered solution Tween 20, and evaluated with the appropriate antibodies (Supplementary Table 1).

PCR Analysis

Total RNA was extracted with TRIzol (Invitrogen, Waltham, MA). RNA (1 μg) was reverse transcribed with the High Capacity cDNA Reverse Transcription Kit (Applied Biosystems, Waltham, MA) and subjected to quantitative real-time PCR (QuantStudio 12K Flex Real-Time PCR System; Thermo Fisher Scientific [RRID SCR_021098]) using QuantiTect SYBR Green Master Mix (QIAGEN, Germantown, MD). Primer sequences are listed in Supplementary Table 2. Mean cycle threshold (CT) values were determined for control and experimental samples. Changes in mRNA expression were normalized to GAPDH mRNA expression with the $2^{-\Delta\Delta CT}$ method.

Statistical Analysis

Data are expressed as means ± SD. Statistical analysis of data with more than two groups were analyzed with two-way ANOVA, and pairwise comparisons were made with the Tukey test for multiple comparisons. Difference between two-groups was determined with unpaired Student *t* test. The relationships between REDD1 expression and blood glucose

levels were tested with Spearman correlation analysis. Significance was defined as $P < 0.05$ for all analyses.

Data and Resource Availability

The data sets and resources generated during this study are available from the corresponding author on reasonable request.

RESULTS

REDD1 Mediates Diabetes-Induced Renal Hypertrophy and Albuminuria

After 16 weeks of STZ diabetes, REDD1 mRNA abundance was increased in kidney tissue homogenates in coordination with fasting blood glucose concentrations (Fig. 1*A*). A corresponding increase in REDD1 protein expression was observed in kidney tissue homogenates from diabetic mice as compared with nondiabetic controls (Fig. 1*B*). Negligible REDD1 mRNA was detected in the glomeruli of nondiabetic mice by ISH, whereas enhanced staining was observed throughout the kidney cortex of diabetic mice (Fig. 1*C*). For evaluation of a role for REDD1 in diabetes-induced renal damage, mice with a germline disruption of REDD1 were administered STZ. Following 16 weeks of diabetes, diabetic and nondiabetic REDD1 KO mice exhibited fasting blood glucose concentrations similar to those observed in diabetic and nondiabetic WT mice (Fig. 2*A*). Diabetes enhanced REDD1 mRNA (Fig. 2*B*) and protein (Fig. 2*C*) expression in the kidney of WT mice. Diabetic WT and REDD1 KO mice had reduced body weights as compared with nondiabetic mice after 16 weeks of STZ diabetes. However, there was no difference in body weight with WT versus REDD1 KO mice (Fig. 2*D*). In WT mice, diabetes increased kidney weight (Fig. 2*E*) and kidney–to–body weight ratio (Fig. 2*F*). As compared with diabetic WT mice, diabetic REDD1 KO mice exhibited reduced kidney weight and kidney–to–body weight ratio. In support of renal hypertrophy, rpS6 phosphorylation was enhanced in STZ diabetic WT mice (Supplementary Fig. 1); however, diabetes did not alter rpS6 phosphorylation in REDD1 KO mice. Urine volumes collected from diabetic WT and REDD1 KO mice were significantly higher as compared with their respective nondiabetic controls (Fig. 2*G*). Urinalysis of diabetic WT mice showed an increased urinary protein band at 60 kDa (Fig. 2*H*) and elevated urinary albumin (Fig. 2*I*). Diabetic mice also exhibited a reduction in urinary creatine concentration (Fig. 2*J*) and increased urinary albumin–to–creatinine ratio (ACR) (Fig. 2*K*). REDD1 deletion prevented proteinuria and normalized urinary ACR in diabetic mice.

Diabetes-Induced Renal Pathology Required REDD1

Glomerular structure (Fig. 3*A*, panels *a–d*) and mesangial proliferation (Fig. 3*A*, panels *e–h*) were examined with H-E and PAS staining, respectively. Histologic examination revealed glomerular hypertrophy, basement membrane thickening, and mesangial proliferation in diabetic WT mice as compared with nondiabetic controls. Increased GV (Fig. 3*B*) and compressed Bowman capsule were observed in diabetic WT mice. Mesangial expansion was also observed within glomeruli of diabetic WT mice (Fig. 3*C*). Features of renal pathology were significantly attenuated or absent in diabetic REDD1 KO mice. In particular, GV and mesangial index were reduced in diabetic REDD1 KO mice as compared with diabetic WT mice. REDD1 deletion also decreased matrix deposition in diabetic mice, evidenced by reduced fibronectin expression (Fig. 3*A*, panels *i–l*, and Fig. 3*D*). Expression of mRNAs encoding profibrotic markers TGF-β1, α-SMA, fibronectin, and collagen 1A1 were enhanced in the kidney of diabetic WT mice as compared with nondiabetic controls, whereas the mRNA encoding the tight junction protein E-cadherin was reduced (Fig. 3*E*). Fibrotic markers were reduced, and E-cadherin expression was increased, in the kidney of diabetic REDD1 KO mice as compared with diabetic WT mice.

REDD1 Contributes to Diabetes-Induced Podocytopenia

Hyperglycemia-induced podocyte loss has previously been reported in cell cultures and rodent models of diabetes (12,27). WT-1 immunolabeling was used to identify podocytes. WT-1 is essential for renal development as well as maintaining the differentiated state of podocytes in the adult kidney (28). A decrease in WT-1–positive cells was observed in glomeruli from diabetic WT mice (Fig. 4*A*). However, REDD1 deletion prevented reduced WT-1 expression in diabetic mice (Fig. 4*B*). A role for REDD1 in podocytopenia was also supported by reduced expression of the podocyte marker podocin in kidney homogenates from diabetic WT mice but not diabetic REDD1 KO mice (Fig. 4*C*). Normal podocyte architecture with filtration slits and evenly spaced slit diaphragms were observed in electron micrographs of renal tissue from nondiabetic mice (Fig. 4*D*). By contrast, glomerular basement membrane thickening and foot process effacement with distancing of slit pores were observed diabetic WT mice. In contrast with diabetic WT mice, podocyte architecture was preserved in diabetic REDD1 KO mice. For investigation of a role for REDD1 in human podocytes, CIHP cells were exposed to hyperglycemic culture conditions, which increased both REDD1 mRNA (Fig. 4*E*) and protein (Fig. 4*F*) expression. Metabolic viability assessment using MTT showed reduced viability of WT podocytes after 24–48 h of exposure to hyperglycemic conditions (Fig. 4*G*). However, hyperglycemic conditions did not reduce viability of REDD1-deficient podocytes. Hyperglycemic conditions also increased cleaved caspase 3 expression in WT, but not in REDD1 KO, podocytes (Fig. 4*H*).

REDD1 Contributes to Oxidative Stress in the Kidney of Diabetic Mice

Increased ROS levels were observed in kidney homogenates from diabetic mice (Fig. 5*A*). Protein oxidation identified by nitrotyrosine immunolabeling was also elevated

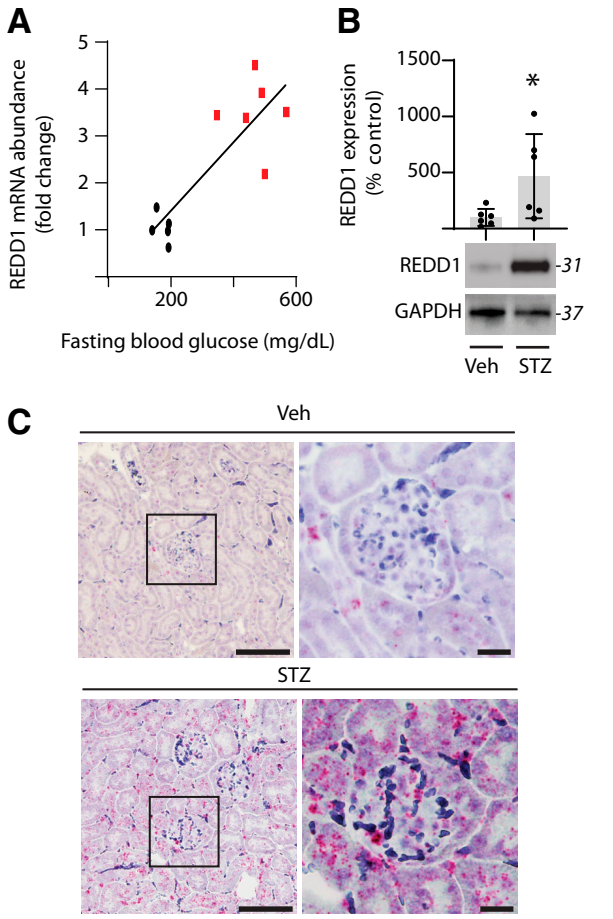

Figure 1—Diabetes promoted renal REDD1 expression. Diabetes was induced in mice with STZ. All analyses were performed 16 weeks after mice were administered STZ or a vehicle (Veh). *A*: REDD1 mRNA abundance in kidney tissue homogenates positively correlated with fasting blood glucose concentrations (Pearson $r = 0.8452$). *B*: REDD1 and GAPDH protein expression was assessed in kidney tissue homogenate with Western blotting. Representative blots are shown. Molecular mass in kDa is indicated at right of each blot. REDD1 expression relative to GAPDH was quantified. Values are presented as means ± SD. Statistical significance was assessed with Student *t* test and is denoted as $*P < 0.05$ vs. vehicle. *C*: REDD1 mRNA (red) was detected in FFPE renal sections by RNA ISH. Representative micrographs at low (×200, scale bar 100 μm) and high (×600, scale bar 20 μm) magnification are shown.

in the kidney of diabetic mice (Fig. 5*B* and *C*). Both ROS levels and nitrotyrosine labeling were reduced in the kidney of diabetic REDD1 KO mice as compared with diabetic WT mice. Exposure to hyperglycemic culture media also enhanced ROS levels in WT podocytes; however, high glucose–induced ROS were not observed in REDD1 KO podocytes (Fig. 5*D* and *E*). To assess the impact of REDD1 on the Nrf2-mediated antioxidant response, an Nrf2 ARE-luciferase reporter was expressed in podocytes. Exposure to hyperglycemic conditions reduced Nrf2 activity in WT cells (Fig. 5*F*). REDD1 KO podocytes exhibited enhanced Nrf2 activity as compared with WT podocytes, and the suppressive effect of hyperglycemic conditions on Nrf2 required REDD1. Examination of Nrf2 target mRNA transcript (i.e., GCLC, GCLM, HO-1, and NQO1) expression was consistent with constitutive activation of Nrf2 in the absence of REDD1 (Fig. 5*G*).

REDD1-Dependent Activation of GSK3β Contributes to Diabetic Nephropathy

We previously demonstrated that REDD1-dependent GSK3β activation contributes to Nrf2 suppression in the retina of diabetic mice (18). In the kidney of diabetic WT mice, we observed a reduction in the inhibitory phosphorylation of GSK3β at Ser9 (Fig. 6*A–B*). The suppressive effect of diabetes on GSK3β phosphorylation was absent in REDD1 KO mice, and GSK3β phosphorylation was increased in diabetic REDD1 KO mice as compared with diabetic WT mice. Similarly, GSK3β phosphorylation was reduced in WT podocytes on exposure to hyperglycemic conditions, and REDD1 was required for this effect (Fig. 6*C*). Together, the observations support REDD1-dependent activation of GSK3β in response to diabetes/hyperglycemic conditions. For examination of the role of GSK3β, GSK3 activity was inhibited using VP3.15. In podocytes exposed to hyperglycemic conditions, VP3.15 reduced glycogen synthase phosphorylation (Supplementary Fig. 2*A*) and attenuated ROS levels (Fig. 6*D*). Moreover, GSK3β inhibition attenuated hyperglycemia-induced loss of podocyte viability (Fig. 6*E*). For determination of the benefits of GSK3β suppression on renal defects, 13 weeks after STZ administration diabetic mice were administered VP3.15 daily for 3 weeks (Supplementary Fig. 2*B*). VP3.15 did not alter body weight (Supplementary Fig. 2*C*). Efficacy of the treatment was confirmed by reduced glycogen synthase phosphorylation in renal tissue lysates of diabetic mice (Supplementary Fig. 2*D*). In diabetic mice receiving VP3.15, renal hypertrophy (Supplementary Fig. 2*E* and *F*) and urinary proteins (Supplementary Fig. 2*G*) were reduced. Evidence for improved renal function was suggested by a trend toward lower urine ACR in diabetic mice receiving VP3.15 as compared with DMSO vehicle ($P = 0.1276$) (Supplementary Fig. 1*H–J*). Importantly, GSK3β inhibition prevented diabetes-induced ROS in kidney homogenates (Fig. 6*F*). GSK3β inhibition also prevented diabetes-induced podocyte loss (Fig. 6*G* and *H*) and attenuated podocyte apoptosis in diabetic mice, as assessed according to colocalization of WT-1– and TUNEL-positive cells (Fig. 6*G* and *I* and Supplementary Fig. 3).

DISCUSSION

Herein, we examined a role for REDD1 in the development of renal complications in a well-characterized preclinical model of type 1 diabetes. REDD1 induction was observed in the kidney of STZ diabetic mice, as well as in human podocytes exposed to hyperglycemic conditions. Diabetes-induced mesangial expansion, matrix deposition, and glomerular ultrastructural alternations were relieved in REDD1 KO mice. Single-cell sequencing supports that REDD1 expression is not localized to a particular cell type

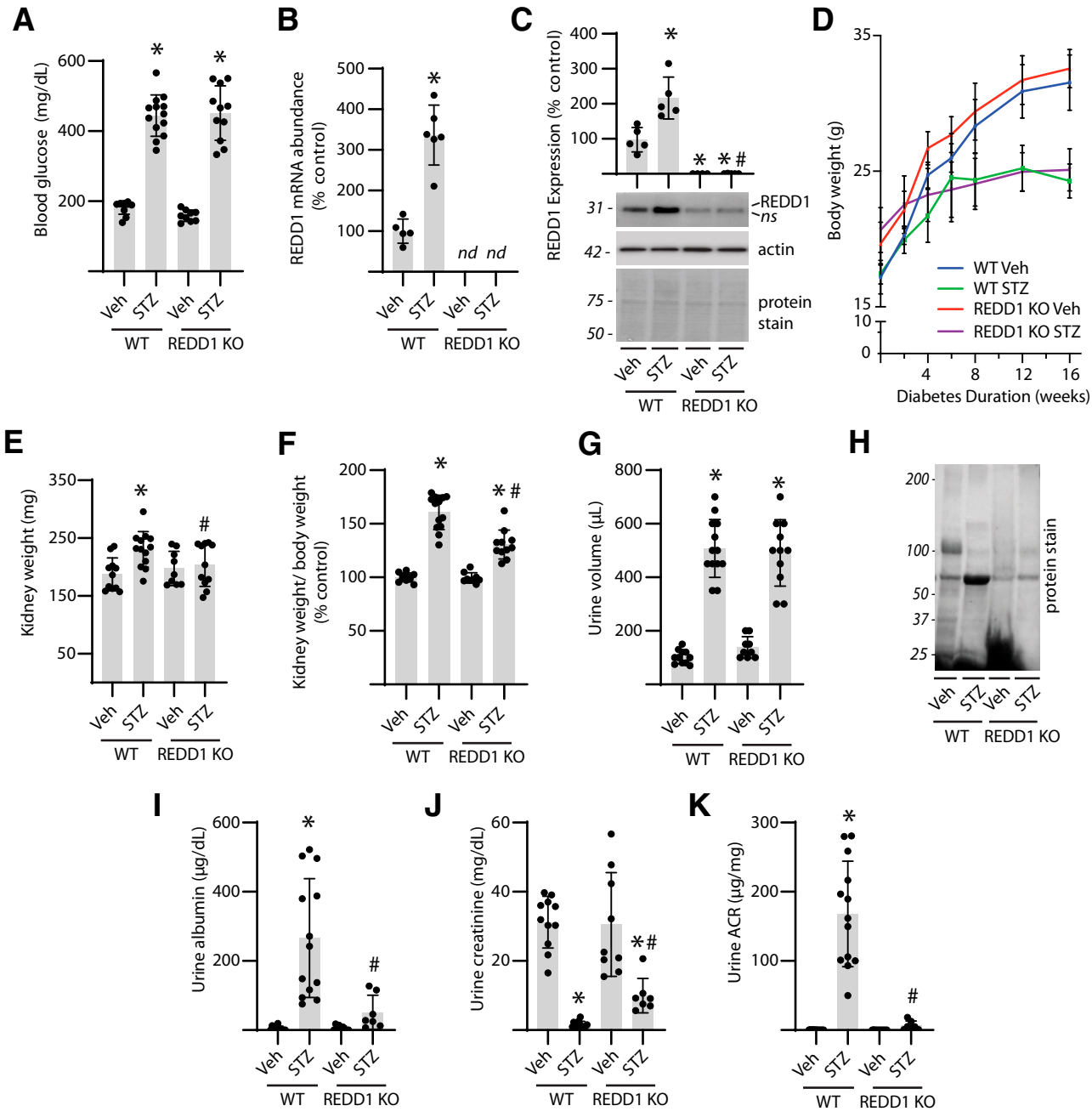

Figure 2—REDD1 was required for renal defects in diabetic mice. Diabetes was induced in WT and REDD1 KO mice with STZ. All analyses were performed 16 weeks after mice were administered STZ or vehicle (Veh). *A*: Fasted blood glucose concentrations were evaluated. *B*: REDD1 mRNA abundance was measured by quantitative PCR. *C*: REDD1 and actin protein expression was assessed in kidney tissue homogenate with Western blotting. Equal gel loading was determined by protein staining. Representative blots are shown. Protein molecular mass is indicated at left of each blot. *D–F*: Body (*D*) and kidney (*E*) weights were determined and renal hypertrophy was characterized as the ratio of kidney weight to body weight (*F*). *G–K*: Urine volume was determined (*G*), and urinary proteins were separated by SDS-PAGE and visualized by protein staining (*H*). Urinary albumin (*I*) and creatinine (*J*) levels were measured with ELISA, and albuminuria was characterized as urine albumin-to-creatinine ratio (ACR) (*K*). Data are presented as means ± SD. Statistical significance is denoted as **P* < 0.05 vs. vehicle, #*P* < 0.05 vs. WT. nd, not detected.

within the kidney (29). REDD1 was initially identified as a stress response gene that was transcriptionally induced in response to hypoxia and oxidative stress (30) but subsequently shown to be elevated in response to cellular stressors including nutrient deprivation and endoplasmic reticular stress (31,32). Increased REDD1 mRNA expression in the renal cortex of diabetic mice supports transcriptional upregulation of REDD1 with STZ diabetes. The studies here also provide evidence that REDD1 acts to promote renal oxidative stress via GSK3β-dependent suppression of the Nrf2 antioxidant response. Overall, the findings support a model wherein diabetes-induced

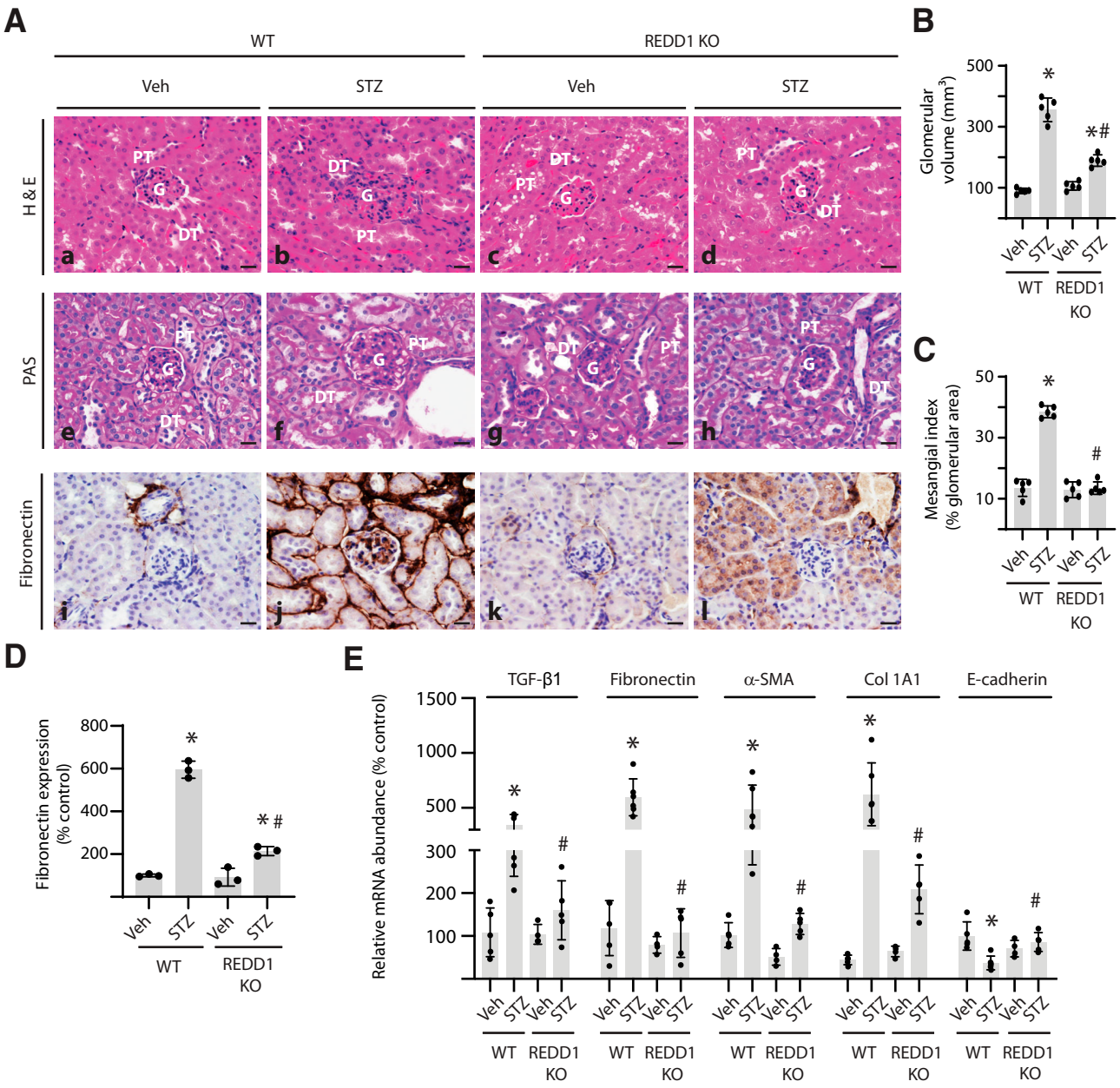

Figure 3—REDD1 ablation ameliorated renal pathology in diabetic mice. Diabetes was induced in WT and REDD1 KO mice by administration of STZ. All analyses were performed 16 weeks after mice were administered STZ or vehicle (Veh). *A*: Renal pathology was examined with H-E (*A–D*) and PAS (*E–H*) staining. Representative micrographs are shown. GV (*B*) and mesangial expansion (*C*) were quantified from PAS sections ($n = 5$) (20–50 glomeruli per mouse). Renal fibrosis was characterized by immunolabeling for fibronectin (*A*, panels *i–l*). *D*: Fibronectin expression in *A* was quantified. *E*: mRNA abundance of profibrotic markers relative to GAPDH was quantified with quantitative PCR. Data are presented as means ± SD. Statistical significance is denoted as $*P < 0.05$ vs. vehicle, $\#P < 0.05$ vs. WT STZ. Micrograph magnification ×600; scale bar 20 μm. DT, distal tubule; G, glomerulus; PT, proximal tubule.

renal REDD1 causes glomerular podocyte damage through disrupted redox homeostasis (Fig. 7).

Microalbuminuria is an important indicator of DN progression and often caused by the dysfunction of the glomerular filtration barrier (33). Podocytes are a core component of this filtration barrier and play a central role in maintaining glomerular structural and functional integrity. Podocyte injury is a key factor in DN progression, with foot process effacement, detachment from the glomerular basement membrane, and podocyte apoptosis often observed in the earliest stages of disease (34,35). Disrupted glomerular architecture, foot process effacement, distancing of slit pores, and podocytopenia were observed in diabetic mice. Remarkably, markers of podocyte dysfunction were absent or reduced in the kidney of diabetic REDD1 KO mice and renal barrier function was preserved.

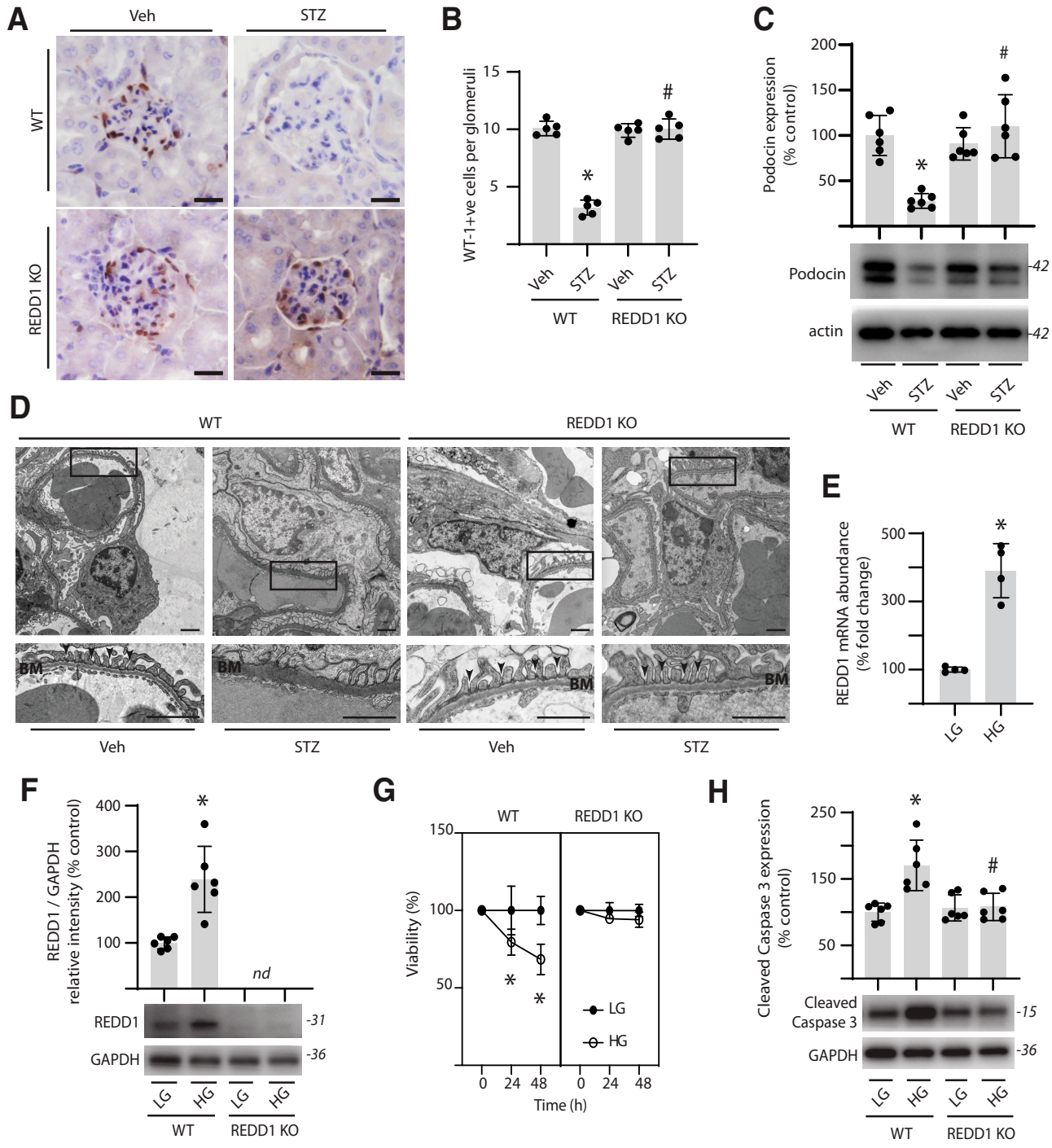

Figure 4—REDD1 deletion prevented diabetes-induced podocytopenia. *A–D*: Diabetes was induced in WT and REDD1 KO mice by administration of STZ. All analyses were performed 16 weeks after mice were administered STZ or vehicle (Veh). *A*: Kidney sections were immunolabeled for WT-1. Representative micrographs are shown (×600 magnification; scale bar 20 μm). *B*: WT-1–positive (WT-1+ve) cells per glomeruli (n = 5; 20 glomeruli per kidney) in *A* were quantified. *C*: Podocin and actin protein expression in the kidney were determined by Western blotting. Representative blots are shown. Protein molecular mass in kDa is indicated at the right of the blots. *D*: Representative photomicrographs from transmission electron microscopy of podocytes are shown (scale bar 2 μm). Foot process with slit diaphragms (arrow heads) and glomerular basement membrane (BM) are indicated. *E–H*: WT and REDD1 KO conditionally immortalized human podocytes were differentiated for 10 days and then exposed to medium containing either 30 mmol/L glucose media (HG) or 5 mmol/L glucose plus 25 mmol/L mannitol (LG) for 0–48 h. REDD1 mRNA abundance (*E*) and protein expression (*F*) were examined with quantitative PCR and Western blotting, respectively. Podocyte metabolic viability was determined with MTT assay (*G*) (n = 6). Cleaved caspase 3 and GAPDH expression were assessed with Western blotting (*H*). Data are presented as means ± SD, and statistical significance is denoted as *$P < 0.05$ vs. vehicle or LG, #$P < 0.05$ vs. WT. nd, not detected.

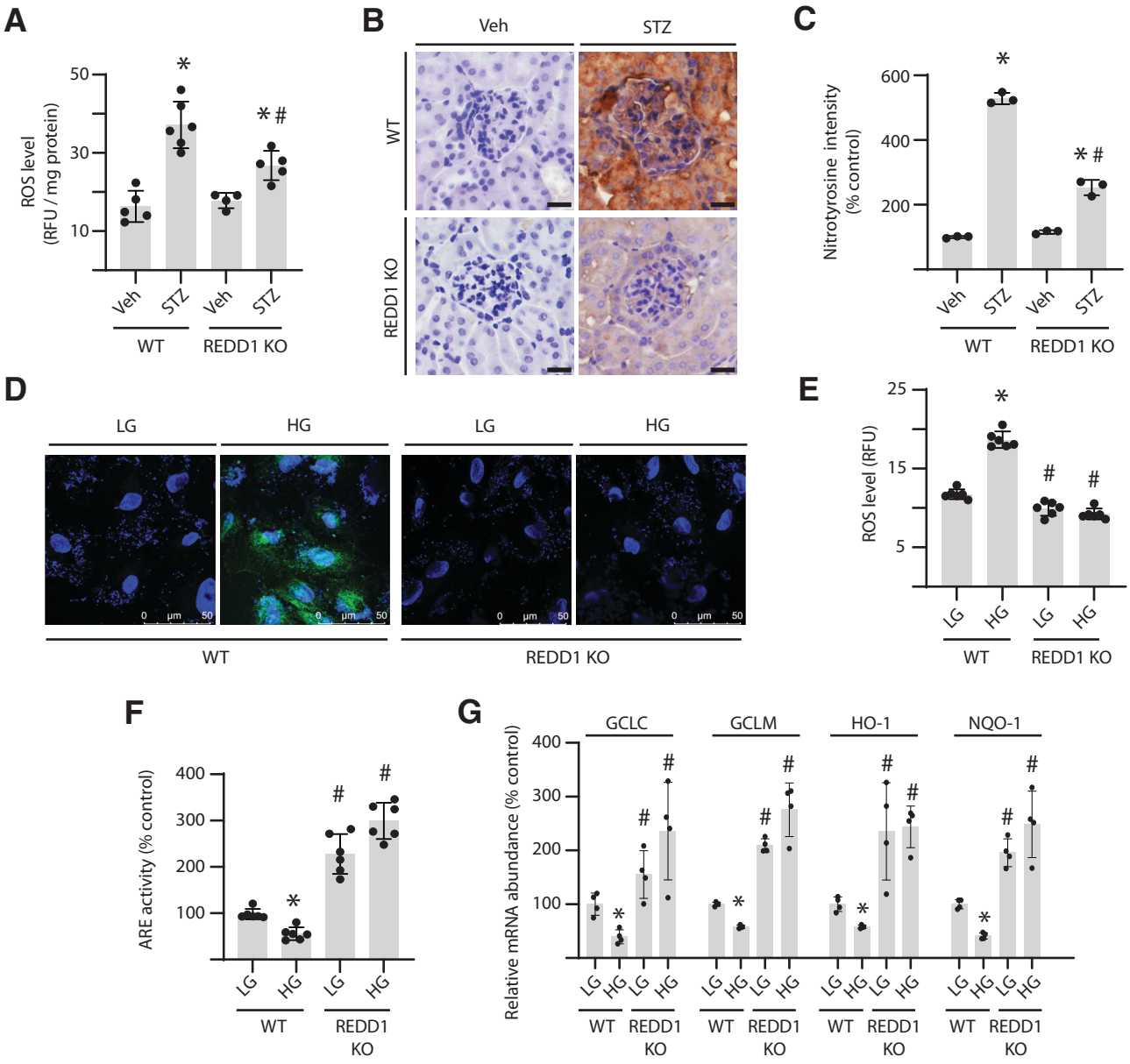

Figure 5—REDD1 deletion inhibited oxidative stress in response to hyperglycemic conditions. *A–C*: Diabetes was induced in WT and REDD1 KO mice with STZ. All analyses were performed 16 weeks after mice were administered STZ or a vehicle (Veh). *A*: ROS levels were determined in kidney homogenate with DCF fluorescence. *B* and *C*: Protein oxidation in renal sections was determined with nitrotyrosine immunolabeling. Representative sections are shown (*B*) (scale bar 20 μm), and nitrotyrosine expression was quantified (*C*). *D–G*: WT and REDD1 KO podocytes were exposed to medium containing 30 mmol/L glucose (HG) or 5 mmol/L glucose plus 25 mmol/L mannitol (LG) for 48 h. ROS were visualized with DCFDA (scale bar 50 μm) (*D*), and DCF fluorescence intensity was quantified (*E*). *F*: Nrf2 activity was measured in cells expressing an ARE luciferase reporter. *G*: mRNA expression of Nrf2 gene targets was quantified with quantitative PCR. Data are presented as means ± SD, and statistical significance is denoted as $*P < 0.05$ vs. vehicle or LG, $\#P < 0.05$ vs. WT. RFU, relative fluorescence units.

Hyperglycemia is a major determinant of podocytopenia and DN progression (12,36). Podocyte cultures exposed to conditions including elevated glucose concentrations undergo apoptosis due to activation of p38 MAPK and classical caspase 3 signaling (12). A role for REDD1 in high glucose–induced caspase activation and cell death was previously demonstrated in R28 neuronal precursor cells (15). In support of that observation, we found that REDD1 deletion prevented an increase in cleaved caspase 3 expression and reduced viability in human podocyte cultures exposed to hyperglycemic conditions. The principle pathways responsible for hyperglycemia-induced tissue damage are all linked to the overproduction of ROS (37). An imbalance between ROS production and the cellular antioxidant response leads to development of oxidative stress, which is a key driver of DN pathology (38–40). Combating oxidative stress with antioxidant adjuvant therapies has been successful in delaying if not preventing the

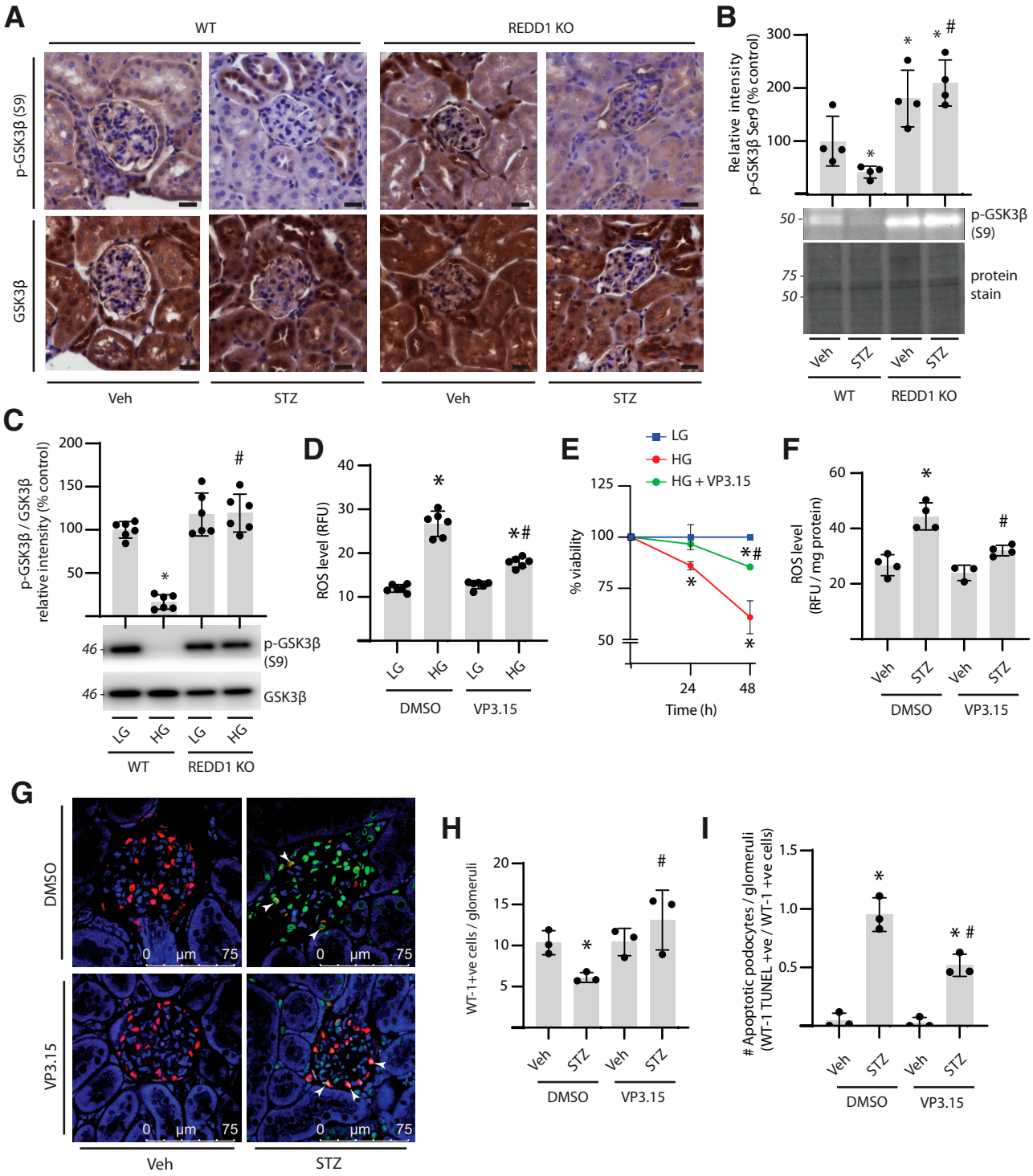

Figure 6—REDD1-dependent GSK3 activation contributes to diabetes-induced oxidative stress and renal defects. *A* and *B* and *F–I*: Diabetes was induced in WT or REDD1 KO mice with STZ. All analyses were performed 16 weeks after mice were administered STZ or vehicle (Veh). GSK3β phosphorylation at Ser9 was examined in renal sections (*A*) and kidney homogenates (*B*) by immunolabeling and Western blotting, respectively. Representative blots are shown. *C–E*: WT or REDD1 KO podocytes were exposed to medium containing 30 mmol/L glucose (HG) or 5 mmol/L glucose plus 25 mmol/L mannitol (LG) for 48 h. GSK3β phosphorylation at Ser9 was examined in cell lysates with Western blotting (*C*). ROS levels were determined in podocytes with DCF fluorescence (*D*). Podocyte metabolic viability was determined with MTT assay (*E*) (n = 5). *F–I*: During the last 3 weeks of diabetes, mice were treated daily with VP3.15 or a vehicle control (DMSO). ROS levels in kidney tissue lysates were examined with DCF fluorescence (*F*). WT1 (red) colocalization with TUNEL-positive cells (green) was determined with immunofluorescence (*G*). Representative micrographs are shown (×600 magnification; scale bar 75 μm), and number of WT-1–positive (WT-1+ve) cells per glomeruli (n = 3; 20 glomeruli per kidney) was quantified (*H*). The number of apoptotic podocytes within glomeruli (arrowhead in *G*) was quantified (*I*). Data are presented as means ± SD. Statistical significance is denoted as *$P <$ 0.05 vs. vehicle or LG, #$P < 0.05$ vs. DMSO. p-, phosphorylated; RFU, relative fluorescence units.

development of DN pathologies in preclinical rodent models (41,42). In clinical studies, antioxidant supplementation consistently improves albuminuria (43). Enhanced REDD1 expression is associated with multiple disease models in which oxidative stress is a driver of pathology (44). In the retina of diabetic mice and in retinal cell cultures exposed to hyperglycemic conditions, REDD1 contributes to the development of oxidative stress (15,17). Moreover, multiple reports have implicated hyperglycemia-induced oxidative stress as a trigger for cell death mechanisms including apoptosis (12,15,36,45). In the current study, REDD1 deletion blunted oxidative stress in the kidney of diabetic mice and in human podocytes exposed to hyperglycemic conditions.

The transcription factor Nrf2 regulates expression of >200 antioxidant response genes by binding to an ARE enhancer region of their promoters (45,46). Nrf2 is classically regulated by the adaptor protein Kelch-like ECH-associated protein 1 (Keap1), which facilitates proteasomal degradation of the transcription factor. When ROS accumulate, cysteine residues on Keap1 become oxidized and Nrf2 is allowed to translocate into the nucleus to promote the production of antioxidants (47). In addition, GSK3β directly phosphorylates Nrf2 to promote its nuclear exclusion and degradation by a protein cluster containing the ubiquitin ligase adapter β-transducin repeat–containing protein (β-TrCP) (48). In human podocytes exposed to hyperglycemic conditions, ROS levels were enhanced in coordination with suppression of Nrf2 activity. REDD1 deletion prevented the suppressive effect of hyperglycemic conditions on Nrf2 activity, and also podocytes lacking REDD1 exhibited chronic hyperactivation of Nrf2. Previous work from our laboratory provides evidence that REDD1 acts to suppress Nrf2 activity by promoting GSK3-dependent proteasomal degradation of the transcription factor (18).

Diabetes-induced GSK3β activation is observed in various tissues including the kidney (21). In the glomerulus, GSK3β is an evolutionarily conserved, redox-sensitive serine/threonine protein kinase that is predominantly expressed in podocytes (49,50). GSK3β expression in podocytes serves as a critical regulator of kidney function, injury, and repair (49,50). REDD1 promotes GSK3β activation via suppression of the protein kinase Akt. More specifically, REDD1 mediates dephosphorylation of Akt at Thr308

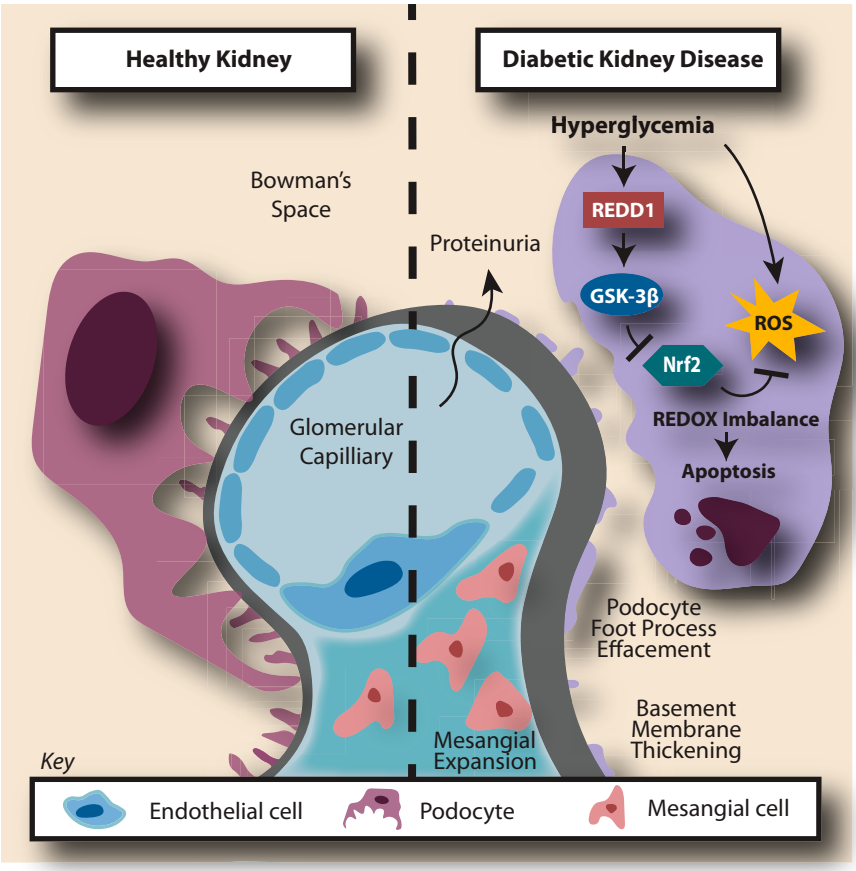

Figure 7—REDD1 contributes to diabetes-induced podocyte injury and renal complications. Diabetes and hyperglycemic conditions enhanced REDD1 to promote GSK3β signaling and inhibit the Nrf2 antioxidant response in podocytes. Chronic oxidative insult results in altered renal pathology stemming from podocyte apoptosis, including glomerular basement membrane thickening and foot process effacement. Diabetes-induced podocyte loss compromises renal filtration function resulting in macroalbuminuria.

via recruitment of the protein phosphatase 2A, resulting in attenuated Akt activation (20). Akt phosphorylates the N-terminus of GSK3β at Ser9, which reduces GSK3β kinase activity by obstructing substrate recognition (51). In the retina of diabetic mice, REDD1 protein expression is enhanced and necessary for attenuated GSK3β phosphorylation (17). Data presented here extend from these studies in demonstrating that REDD1 was necessary for suppression of GSK3β phosphorylation in both the kidney of diabetic mice and in podocytes exposed to hyperglycemic conditions. GSK3 inhibitors have been successfully used to prevent deficits in renal function and cardiac remodeling in rodent models of diabetes and diabetic ischemia reperfusion injury (22,52,53). Herein, benefits of REDD1 deletion in the prevention of DN pathology were recapitulated by GSK3 inhibition. We found that administration of a GSK3 inhibitor to diabetic mice reduced kidney hypertrophy, normalized ROS levels, and attenuated podocyte loss.

Mechanisms underlying compensatory kidney hypertrophy are not well characterized but are thought to involve hyperactivation of the protein kinase mTOR (mechanistic target of rapamycin) in complex 1 (mTORC1) (54). Activation of mTORC1 enhances phosphorylation of rpS6, promoting cell growth and proliferation in response to nutrients and growth factors. Rheb-GTP is an obligate activator of mTORC1, and insulin binding to its receptor promotes Rheb-GTP loading (55,56). REDD1 acts as a dominant regulator of mTORC1 signaling and suppresses mTORC1 kinase activity by reducing Rheb-GTP (20). In support of the prior report (57), we observed enhanced phosphorylation of rpS6 in the kidney of STZ diabetic mice, which is consistent with activation of mTORC1. In nondiabetic REDD1 KO mice, rpS6 phosphorylation in the kidney was enhanced as compared with nondiabetic WT mice, and there was no change with STZ diabetes. Consequently, rpS6 phosphorylation was similar in diabetic WT and diabetic REDD1 KO mice. The findings suggest that REDD1 expression may contribute to rpS6 phosphorylation in the kidney of nondiabetic mice but do not support REDD1-dependent mTORC1 suppression in the context of diabetes. Upregulation of mTORC1 signaling in the context of diabetes is paradoxical, as both insulin deficiency and increased REDD1 expression should act counter to its activation. One possibility is that diabetes promotes mTORC1 activation despite a relative reduction in Rheb-GTP. This could potentially be accomplished by enhanced lysosomal localization of mTORC1, as is seen with amino acid signaling (58,59).

Overall, the findings provide new insight into the mechanism whereby type 1 diabetes and hyperglycemic conditions contribute to the development of renal complications. At present, whether REDD1 plays a similar role in the development of renal damage in type 2 diabetes is not known. However, REDD1 expression is upregulated in skeletal muscle of both patients with type 2 diabetes (60) and rodent models of obesity (61), and evidence supports a role for the protein in development of insulin resistance. In the kidney of STZ diabetic mice, REDD1 expression was increased and GSK3β phosphorylation was decreased concomitant with podocytopenia and renal injury. However, REDD1 deletion reduced oxidative stress in the kidney of diabetic mice and prevented both podocyte loss and the resulting glomerular filtration defects. The data are consistent with a mechanism wherein a REDD1/GSK3β signaling axis acts to negatively regulate redox homeostasis in the podocytes resulting in podocytopenia and albuminuria. These proof-of-concept studies support the possibility that therapeutic intervention to repress REDD1 expression in the kidney may offer hope for maintaining renal function in patients with diabetes.

Acknowledgments. The authors thank Dr. Elena Feinstein (Quark Pharmaceuticals) for permission to use the REDD1 KO mice. The preparation of histology sections and H-E staining of tissue sections, carried out by Ellen Mullady and Gretchen Snavely, Department of Comparative Medicine, Penn State College of Medicine, are greatly appreciated.

Funding. This research was supported by the American Diabetes Association Pathway to Stop Diabetes grant 1-14-INI-04, National Institutes of Health grants R01 EY029702 and R01 EY032879 (to M.D.D.), and a Children's Miracle Network Hospitals Trainee Research Grant (to S.S.).

Duality of Interest. No potential conflicts of interest relevant to this article were reported.

Author Contributions. S.S., S.R.K, and M.D.D. contributed to study conceptualization. S.S., E.I.Y., A.L.T., and M.D.D. contributed to data curation. S.S., E.I.Y., A.L.T., and M.D.D. contributed to formal analysis. S.S. and M.D.D. acquired funding. S.S., E.I.Y., A.L.T., W.P.M., and H.C. performed the investigation. S.S. and M.D.D. visualized the data. S.S., H.C., K.H., S.R.K., and M.D.D. contributed to development of study methodology. S.S. and M.D.D. contributed to writing the manuscript. S.S., E.I.Y., A.L.T., W.P.M., K.H., S.R.K., and M.D.D. reviewed and edited the manuscript. K.H., S.R.K., and M.D.D. provided resources. S.R.K. and M.D.D. supervised the study. M.D.D. is the guarantor of this work and, as such, had full access to all the data in the study and takes responsibility for the integrity of the data and the accuracy of the data analysis.

Prior Presentation. Parts of this study were presented in abstract form at the 2022 Experimental Biology annual meeting, Philadelphia, PA, 2–5 April 2022.

References

1. Cheng HT, Xu X, Lim PS, Hung KY. Worldwide epidemiology of diabetes-related end-stage renal disease, 2000–2015. Diabetes Care 2021;44:89–97

2. Lachin JM, Genuth S, Cleary P, Davis MD; Diabetes Control and Complications Trial/Epidemiology of Diabetes Interventions and Complications Research Group. Retinopathy and nephropathy in patients with type 1 diabetes four years after a trial of intensive therapy. N Engl J Med 2000;342:381–389

3. Abdel-Rahman EM, Saadulla L, Reeves WB, Awad AS. Therapeutic modalities in diabetic nephropathy: standard and emerging approaches. J Gen Intern Med 2012;27:458–468

4. Yamazaki T, Mimura I, Tanaka T, Nangaku M. Treatment of diabetic kidney disease: current and future. Diabetes Metab J 2021;45:11–26

5. Vallon V, Komers R. Pathophysiology of the diabetic kidney. Compr Physiol 2011;1:1175–1232

6. Pavenstädt H. Roles of the podocyte in glomerular function. Am J Physiol Renal Physiol 2000;278:F173–F179
7. Pagtalunan ME, Miller PL, Jumping-Eagle S, et al. Podocyte loss and progressive glomerular injury in type II diabetes. J Clin Invest 1997;99: 342–348
8. Steffes MW, Schmidt D, McCrery R; International Diabetic Nephropathy Study Group. Glomerular cell number in normal subjects and in type 1 diabetic patients. Kidney Int 2001;59:2104–2113
9. Fujita Y, Tominaga T, Abe H, et al. An adjustment in BMP4 function represents a treatment for diabetic nephropathy and podocyte injury. Sci Rep 2018;8:13011
10. Lee HS, Suh JY, Kang BC, Lee E. Lipotoxicity dysregulates the immunoproteasome in podocytes and kidneys in type 2 diabetes. Am J Physiol Renal Physiol 2021;320:F548–F558
11. Eid AA, Gorin Y, Fagg BM, et al. Mechanisms of podocyte injury in diabetes: role of cytochrome P450 and NADPH oxidases. Diabetes 2009;58:1201–1211
12. Susztak K, Raff AC, Schiffer M, Böttinger EP. Glucose-induced reactive oxygen species cause apoptosis of podocytes and podocyte depletion at the onset of diabetic nephropathy. Diabetes 2006;55:225–233
13. Horak P, Crawford AR, Vadysirisack DD, et al. Negative feedback control of HIF-1 through REDD1-regulated ROS suppresses tumorigenesis. Proc Natl Acad Sci U S A 2010;107:4675–4680
14. Qiao S, Dennis M, Song X, et al. A REDD1/TXNIP pro-oxidant complex regulates ATG4B activity to control stress-induced autophagy and sustain exercise capacity. Nat Commun 2015;6:7014
15. Miller WP, Yang C, Mihailescu ML, et al. Deletion of the Akt/mTORC1 repressor REDD1 prevents visual dysfunction in a rodent model of type 1 diabetes. Diabetes 2018;67:110–119
16. Dai W, Miller WP, Toro AL, et al. Deletion of the stress-response protein REDD1 promotes ceramide-induced retinal cell death and JNK activation. FASEB J 2018;32
17. Miller WP, Toro AL, Barber AJ, Dennis MD. REDD1 activates a ROS-generating feedback loop in the retina of diabetic mice. Invest Ophthalmol Vis Sci 2019;60:2369–2379
18. Miller WP, Sunilkumar S, Giordano JF, Toro AL, Barber AJ, Dennis MD. The stress response protein REDD1 promotes diabetes-induced oxidative stress in the retina by Keap1-independent Nrf2 degradation. J Biol Chem 2020;295:7350–7361
19. Nguyen QD, Schachar RA, Nduaka CI, et al.; DEGAS Clinical Study Group. Dose-ranging evaluation of intravitreal siRNA PF-04523655 for diabetic macular edema (the DEGAS study). Invest Ophthalmol Vis Sci 2012;53:7666–7674
20. Dennis MD, Coleman CS, Berg A, Jefferson LS, Kimball SR. REDD1 enhances protein phosphatase 2A-mediated dephosphorylation of Akt to repress mTORC1 signaling. Sci Signal 2014;7:ra68
21. Liang X, Wang P, Chen B, et al. Glycogen synthase kinase 3β hyperactivity in urinary exfoliated cells predicts progression of diabetic kidney disease. Kidney Int 2020;97:175–192
22. Wan J, Li P, Liu DW, et al. GSK-3β inhibitor attenuates urinary albumin excretion in type 2 diabetic db/db mice, and delays epithelial-to-mesenchymal transition in mouse kidneys and podocytes. Mol Med Rep 2016;14:1771–1784
23. Brafman A, Mett I, Shafir M, et al. Inhibition of oxygen-induced retinopathy in RTP801-deficient mice. Invest Ophthalmol Vis Sci 2004;45:3796–3805
24. Rangan GK, Tesch GH. Quantification of renal pathology by image analysis. Nephrology (Carlton) 2007;12:553–558
25. Saleem MA, O'Hare MJ, Reiser J, et al. A conditionally immortalized human podocyte cell line demonstrating nephrin and podocin expression. J Am Soc Nephrol 2002;13:630–638
26. Dai, W, Miller, WP, Toro, AL, et al. Deletion of the stress-response protein REDD1 promotes ceramide-induced retinal cell death and JNK activation. FASEB J 2018;32: fj201800413RR
27. Lenoir O, Jasiek M, Hénique C, et al. Endothelial cell and podocyte autophagy synergistically protect from diabetes-induced glomerulosclerosis. Autophagy 2015;11:1130–1145
28. Kreidberg JA, Sariola H, Loring JM, et al. WT-1 is required for early kidney development. Cell 1993;74:679–691
29. Miao Z, Balzer MS, Ma Z, et al. Single cell regulatory landscape of the mouse kidney highlights cellular differentiation programs and disease targets. Nat Commun 2021;12:2277
30. Ellisen LW, Ramsayer KD, Johannessen CM, et al. REDD1, a developmentally regulated transcriptional target of p63 and p53, links p63 to regulation of reactive oxygen species. Mol Cell 2002;10:995–1005
31. Kimball SR, Jefferson LS. Induction of REDD1 gene expression in the liver in response to endoplasmic reticulum stress is mediated through a PERK, eIF2α phosphorylation, ATF4-dependent cascade. Biochem Biophys Res Commun 2012;427:485–489
32. Xu D, Dai W, Kutzler L, et al. ATF4-mediated upregulation of REDD1 and Sestrin2 suppresses mTORC1 activity during prolonged leucine deprivation. J Nutr 2020;150:1022–1030
33. Benzing T, Salant D. Insights into glomerular filtration and albuminuria. N Engl J Med 2021;384:1437–1446
34. Li JJ, Kwak SJ, Jung DS, et al. Podocyte biology in diabetic nephropathy. Kidney Int Suppl 2007;72:S36–S42
35. Ziyadeh FN, Wolf G. Pathogenesis of the podocytopathy and proteinuria in diabetic glomerulopathy. Curr Diabetes Rev 2008;4:39–45
36. Paeng J, Chang JH, Lee SH, et al. Enhanced glycogen synthase kinase-3β activity mediates podocyte apoptosis under diabetic conditions. Apoptosis 2014;19:1678–1690
37. Brownlee M. The pathobiology of diabetic complications: a unifying mechanism. Diabetes 2005;54:1615–1625
38. Forbes JM, Coughlan MT, Cooper ME. Oxidative stress as a major culprit in kidney disease in diabetes. Diabetes 2008;57:1446–1454
39. Miranda-Díaz, AG, Pazarín-Villaseñor, L, Yanowsky-Escatell, FG, Andrade-Sierra, J. Oxidative stress in diabetic nephropathy with early chronic kidney disease. J Diabetes Res 2016;2016:7047238
40. Singh DK, Winocour P, Farrington K. Oxidative stress in early diabetic nephropathy: fueling the fire. Nat Rev Endocrinol 2011;7:176–184
41. Odetti P, Pesce C, Traverso N, et al. Comparative trial of N-acetyl-cysteine, taurine, and oxerutin on skin and kidney damage in long-term experimental diabetes. Diabetes 2003;52:499–505
42. Shang G, Tang X, Gao P, et al. Sulforaphane attenuation of experimental diabetic nephropathy involves GSK-3 beta/Fyn/Nrf2 signaling pathway. J Nutr Biochem 2015;26:596–606
43. Bolignano, D, Cernaro, V, Gembillo, G, Baggetta, R, Buemi, M, D'Arrigo, G. Antioxidant agents for delaying diabetic kidney disease progression: a systematic review and meta-analysis. PLoS One 2017;12:e0178699
44. Miller WP, Sunilkumar S, Dennis MD. The stress response protein REDD1 as a causal factor for oxidative stress in diabetic retinopathy. Free Radic Biol Med 2021;165:127–136
45. Miller WP, Toro AL, Sunilkumar S, et al. Müller glial expression of REDD1 is required for retinal neurodegeneration and visual dysfunction in diabetic mice. Diabetes 2022;71:1051–1062
46. Nguyen T, Sherratt PJ, Pickett CB. Regulatory mechanisms controlling gene expression mediated by the antioxidant response element. Annu Rev Pharmacol Toxicol 2003;43:233–260
47. Dinkova-Kostova AT, Holtzclaw WD, Cole RN, et al. Direct evidence that sulfhydryl groups of Keap1 are the sensors regulating induction of phase 2 enzymes that protect against carcinogens and oxidants. Proc Natl Acad Sci USA 2002;99:11908–11913
48. Salazar M, Rojo AI, Velasco D, de Sagarra RM, Cuadrado A. Glycogen synthase kinase-3β inhibits the xenobiotic and antioxidant cell response by direct phosphorylation and nuclear exclusion of the transcription factor Nrf2. J Biol Chem 2006;281:14841–14851

49. Hurcombe JA, Hartley P, Lay AC, et al. Podocyte GSK3 is an evolutionarily conserved critical regulator of kidney function. Nat Commun 2019;10:403
50. Jamadar A, Rao R. Glycogen synthase kinase-3 signaling in acute kidney injury. Nephron 2020;144:609–612
51. Cross DAE, Alessi DR, Cohen P, Andjelkovich M, Hemmings BA. Inhibition of glycogen synthase kinase-3 by insulin mediated by protein kinase B. Nature 1995;378:785–789
52. Wang Y, Feng W, Xue W, et al. Inactivation of GSK-3β by metallothionein prevents diabetes-related changes in cardiac energy metabolism, inflammation, nitrosative damage, and remodeling. Diabetes 2009;58:1391–1402
53. Shen X, Hu B, Xu G, et al. Activation of Nrf2/HO-1 pathway by glycogen synthase kinase-3β inhibition attenuates renal ischemia/reperfusion injury in diabetic rats. Kidney Blood Press Res 2017;42:369–378
54. Puelles VG, van der Wolde JW, Wanner N, et al. mTOR-mediated podocyte hypertrophy regulates glomerular integrity in mice and humans. JCI Insight 2019;4:99271
55. Inoki K, Li Y, Xu T, Guan KL. Rheb GTPase is a direct target of TSC2 GAP activity and regulates mTOR signaling. Genes Dev 2003;17:1829–1834
56. Long X, Lin Y, Ortiz-Vega S, Yonezawa K, Avruch J. Rheb binds and regulates the mTOR kinase. Curr Biol 2005;15:702–713
57. Gödel M, Hartleben B, Herbach N, et al. Role of mTOR in podocyte function and diabetic nephropathy in humans and mice. J Clin Invest 2011;121:2197–2209
58. Sancak Y, Peterson TR, Shaul YD, et al. The Rag GTPases bind raptor and mediate amino acid signaling to mTORC1. Science 2008;320:1496–1501
59. Dennis MD, Baum JI, Kimball SR, Jefferson LS. Mechanisms involved in the coordinate regulation of mTORC1 by insulin and amino acids. J Biol Chem 2011;286:8287–8296
60. Williamson DL, Dungan CM, Mahmoud AM, Mey JT, Blackburn BK, Haus JM. Aberrant REDD1-mTORC1 responses to insulin in skeletal muscle from Type 2 diabetics. Am J Physiol Regul Integr Comp Physiol 2015;309:R855–R863
61. Williamson DL, Li Z, Tuder RM, Feinstein E, Kimball SR, Dungan CM. Altered nutrient response of mTORC1 as a result of changes in REDD1 expression: effect of obesity vs. REDD1 deficiency. J Appl Physiol 2014;117:246–256